

Article

HYSCORE Spectroscopy to Resolve Electron–Nuclear Structure of Vanadyl Porphyrins in Asphaltenes from the Athabasca Oil Sands In Situ Conditions

Margarita A. Sadovnikova, Fadis F. Murzakhanov , Georgy V. Mamin and Marat R. Gafurov * 

Institute of Physics, Kazan Federal University, 18 Kremlevskaya Str., 420008 Kazan, Russia

* Correspondence: marat.gafurov@kpfu.ru; Tel.: +7-(843)-2926480

Abstract: The purpose of this work is to analyze the electron–nuclear interactions of the vanadyl-porphyrin (VP) complexes in oil asphaltenes. Asphaltenes from the Athabasca oil sands were studied by HYperfine Sublevel CORrelation Spectroscopy (HYSCORE) electron paramagnetic resonance (EPR). It makes it possible to resolve and interpret complex hyperfine spectra of intrinsic VP with strong and weak hyperfine interactions between the electron magnetic moment and various nuclear spins (^1H , ^{14}N , ^{51}V). The main parameters of spin-Hamiltonian for the VP spin system are determined. The axially symmetric structure of the VP complexes is revealed, and the local nuclear environment of the paramagnetic center is investigated. The results can be used for the study of asphaltene electron–nuclear structure and asphaltene aggregates with the aim of elucidating asphaltenes' transformation(s) under the influence of external treatment.

Keywords: asphaltenes; electron paramagnetic resonance; vanadyl complexes; HYperfine Sublevel CORrelation Spectroscopy



Citation: Sadovnikova, M.A.; Murzakhanov, F.F.; Mamin, G.V.; Gafurov, M.R. HYSCORE Spectroscopy to Resolve Electron–Nuclear Structure of Vanadyl Porphyrins in Asphaltenes from the Athabasca Oil Sands In Situ Conditions. *Energies* **2022**, *15*, 6204. <https://doi.org/10.3390/en15176204>

Academic Editors: Md Motiur Rahman, Mohamed R. Haroun and Abdulrazag Zekri

Received: 19 July 2022

Accepted: 24 August 2022

Published: 26 August 2022

Publisher's Note: MDPI stays neutral with regard to jurisdictional claims in published maps and institutional affiliations.



Copyright: © 2022 by the authors. Licensee MDPI, Basel, Switzerland. This article is an open access article distributed under the terms and conditions of the Creative Commons Attribution (CC BY) license (<https://creativecommons.org/licenses/by/4.0/>).

1. Introduction

The concentration of metalloporphyrins (mainly the nickel and vanadyl porphyrin (VP) complexes locked in asphaltenes) reach values of ≥ 1000 ppm in heavy oils [1], allowing efficient extraction of nickel and vanadium from the petroleum. Petroleum VP exhibits an extremely extensive structural and elemental diversity [2]. The VP molecule can contain various types of substitutions, including alkyl, cycloalkane, and aromatic groups [3], and is often paramagnetic [4] to be analyzed by electron paramagnetic resonance (EPR) techniques [5]. It is also known that VP can participate in the asphaltenes aggregation [6]. Information about the amount, properties, and structure of petroleum VP is actively used not only for the productive removal of metals from the oil source but also to track the processes of the improved-oil-recovery (IOR) and enhanced-oil-recovery (EOR) [7–11]. It follows that intrinsic petroleum VP can serve as a sensitive signaling molecule(s) to follow IOR and EOR treatments. However, despite the decades of VP and petroleum investigations, such tracking, especially with in situ conditions, is still a challenge [12–16].

The main concern of researchers and technologists is to reduce the viscosity of oil and the amount of asphaltenes aggregates. Deep and effective IOR/EOR implies fundamental knowledge of the structure of the oil constituents and establishing a relationship between their structure and bulk properties. As pointed out above, vanadyl porphyrins are important oil elements that deserve detailed study.

Approximately half of the vanadium (and nickel) porphyrins can be identified and quantified by their characteristic ultraviolet (UV) and visible (vis) spectra. The remaining vanadium- and nickel-containing non-porphyrins species have no distinct UV–vis bands [12]. However, the results of X-ray absorption fine structure (EXAFS) spectroscopy and X-ray absorption near-edge structure (XANES) spectroscopy indicated that these non-porphyrins are indeed still bound in a porphyrinic structure without revealing the charac-

teristic UV–visible absorption. Mass spectroscopy showed that the majority of vanadium and nickel compounds in asphaltenes existed in the form of porphyrins, including alkyl porphyrins, sulfur-containing porphyrins, nitrogen-containing porphyrins, and oxygen-containing porphyrins [7–9]. The porphyrins with O, S, and N atoms should associate more strongly with the asphaltenes than the less polar components. The porphyrins are generally believed to be chelate or non-covalently associated with aromatic asphaltene components by π – π interactions. To sum up, the study of petroleum metal complexes can provide a useful insight into the source of petroleum accumulation, especially when combined with classification parameters derived from molecular, isotopic, and bulk parameters [17].

VP and asphaltenes contain magnetic nuclei, such as ^1H , ^{13}C , ^{14}N , and ^{51}V , providing an excellent opportunity for the use of EPR techniques, which are aimed at analyzing the hyperfine interaction (HFI)—interaction between the electron and nuclear spins, characterized by the parameter A —hyperfine constant [5]. Unfortunately, in oil systems, due to the broad EPR signals and overlapping of signals of diverse origin(s), it is often quite problematic to obtain a read out the A -values for ^1H , ^{13}C , ^{14}N [18,19]. One should apply more elaborated EPR techniques sensitive to the small values of A or their tiny changes during the IOR/EOR treatments. One such approach is the HYperfine Sublevel COReLation Spectroscopy (HYSCORE). This method is based on a 3-pulse Electron Spin Echo Envelope Modulation (ESEEM, see [20,21]) and is described in detail in the section Materials and Methods. The HYSCORE makes it possible to study nuclei with small magnetic moments (having a small value of the gyromagnetic ratio γ), to obtain information about the type of surrounding ligand, corresponding information about the magnitude and mechanism (dipole–dipole or contact Fermi) and determine the parameters of the quadrupole interaction (Q and η) in the case for nuclei with the nuclear spin $I > 1/2$. The method can provide information about the presence of equivalent nuclei, as well as distinguish two types of HFI: with weak coupling $|A| < 2|\nu_{\text{Larmor}}|$ and with strong coupling $|A| > 2|\nu_{\text{Larmor}}|$, where ν_{Larmor} is the corresponding Larmor frequency of nuclei. Thanks to the sensitivity and specificity of the HYSCORE experiment, it is possible to register signals from the first coordination sphere of the studied complex(es) as well as from the second nuclear sphere [22].

Previously, few successful attempts had already been made to apply the HYSCORE to VP investigations. The authors of paper [23] demonstrated the possibility of studying the thermal stability of vanadyl tetrafinylporphyrins embedded in silicon by tracking the HFI values of the ^{13}C , ^{14}N , and ^{29}Si nuclei as a function of the annealing temperature. The interatomic distance calculated from the anisotropic dipole–dipole HFI provides information about the geometry of the complex under study. For example, the absolute value of the HFC V–Si and its sign indicates the formation of a direct chemical bond, meaning that the coordination ions VO^{2+} belong to the SiO_2 matrix. Therefore, it is established that VP during the heat treatment is converted into oxygenated VP by the transfer of the VO^{2+} ion from the porphyrin ring into the mineral matrix. In [24], HYSCORE spectroscopy was applied to follow the changes in the chemical environment of VP in oil samples from various feedstock that have been subjected to hydrotreatment and hydroconversion.

In our paper, for the first time to the best of the authors' knowledge, we apply HYSCORE to the intrinsic for the Athabasca asphaltenes VP complexes to obtain information about the VP electron–nuclear structure. Though the Athabasca asphaltenes have long been well studied by various theoretical and experimental tools [25], including conventional EPR [26] and conventional electron–nuclear double resonance (ENDOR) techniques [27], the vanadyl porphyrins inside the mentioned constituents were not sufficiently investigated in this exceptional complex system [28–31], especially by pulsed EPR techniques. In the course of this work, the main parameters of the spin Hamiltonian (value of the g -factor, the hyperfine interaction constants of both the isotropic and anisotropic parts) were determined with high accuracy. The obtained data allow the suggestion of the planar (axial) structure of vanadyl-porphyrin complexes in asphaltenes.

2. Materials and Methods

The asphaltenes, extracted from the Athabasca oil sands (Athabasca tar sands, Fort McMurray, Buffalo, AB, Canada), were provided by Y.M. Ganeeva (Kazan Scientific Centre of the Russian Academy of Sciences, Kazan, Russia). Table 1 shows some properties of the initial material. Detailed EPR investigation of asphaltenes is described below in section Results and Discussion.

Table 1. Content and element analysis of bitumen from Athabasca oil sands.

S, Mass %	Asphaltenes, Mass %	V, ppm	Ni, ppm
4.0	18	250	100

Four-pulse sequence, as shown in Figure 1a, was exploited using stimulated echo sequence with inverting a 180-degree pulse inserted after the second $\pi/2$ pulse. The application of π pulse leads to a mixing of the nuclear frequencies thanks to the two spin transitions with $m_S = \pm \frac{1}{2}$ of an $S = \frac{1}{2}$ centers. Figure 1b demonstrates the 2 resonance lines of distinctive nucleus emerging at (ν^-, ν^+) and (ν^+, ν^-) in the two-dimensional spectrum. In cases where the nuclear Zeeman frequency is larger than the hyperfine interaction value, the lines appear in the right quadrant. Nuclear frequencies can also occur in the left quadrant for centers with large hyperfine interaction. The HYSORE spectra become more complex for nuclear with quadrupole interaction ($I > 1$) [32].

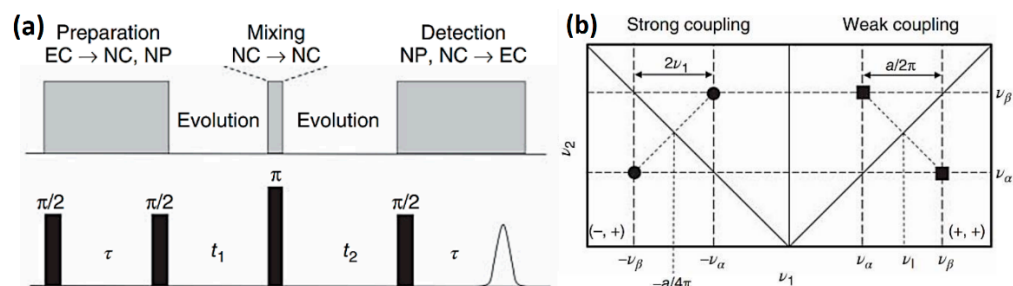


Figure 1. (a) Pulse sequence used to acquire two-dimensional signals from electron–nuclear interactions, where NP—nuclear polarization; NC—nuclear coherences; EC—electron coherences; (b) model of the HYSORE spectra for an $S = \frac{1}{2}$ centers with an anisotropic hyperfine interaction value due to two $I = \frac{1}{2}$ nuclei.

Registration of the two-dimensional time domain spectra carried out by detection of the echo amplitude as a function of pulse delay between t_1 and t_2 (meanwhile with stated τ). The obtained modulation curves are then signal processed by 2D Fourier transformation analysis to extract the resonance lines on the spectra with two frequencies ν_1 and ν_2 directed along the axes. The pulse sequence with each evolution is schematically shown in Figure 1a. The nuclear spin transitions relating to a distinctive species are revealed most easily by a spectra model of the type shown in Figure 1b. The counter map is taken as a projection of the resonance peaks on the frequency layer. Projected points that are symmetrically located at the diagonals in the spectra for an $S = \frac{1}{2}$ species correspond to nuclear spin transitions for the $m_S = +\frac{1}{2}$ and $-\frac{1}{2}$ electronic levels, correspondingly, (denoted α and β) of a nonequivalent nucleus [33].

The experiment was carried out on a Bruker Elexsys E580 commercial spectrometer in the X-band ($\nu = 9.6$ GHz) at a temperature $T = 40$ K. A flow helium cryostat was used to achieve stable low temperatures. HYSORE measurements were made using a 4-pulse sequence $\pi/2-\tau-\pi/2-t_1-\pi-t_2-\pi/2-\tau$ (echo observation) and 4-step phase cycling (to prevent cross-echoes). The amplitude of the echo (signal) was measured as a function of the parameters t_1 and t_2 , each of which was successively increased during the measurement with a step of 16 ns by 128 times. The duration of $\pi/2$ and π pulses was 16 and 32 ns, respectively. The distance between the first and second $\pi/2$ pulses was chosen to be

$\tau = 200$ ns, which corresponds to the optimal value for preventing “blind spots” effects. For further analysis, a two-dimensional Fourier transform was performed and processed in the OriginPro program. The theoretical simulation of EPR spectrum was carried out by EasySpin Matlab software [34].

3. Results

The studied asphaltenes contain two types of different paramagnetic centers: a vanadium complex ($S = 1/2$ and $I = 7/2$ for ^{51}V) and an organic free radical (FR, $S = 1/2$) [35]. Due to the axial symmetry of VO^{2+} (Figure 2a), the presence of a nuclear spin, and the powder (disordered) state of the sample, 16 overlapping resonant transitions are observed in the EPR spectrum due to HFI with ^{51}V . The formation of such splitting for this complex is associated with the presence of an anisotropic hyperfine interaction between the electron shell and the magnetic moment of the ^{51}V vanadium nucleus, where the first eight lines are for parallel, and the remaining eight are for perpendicular orientation. The free radical in the spectrum appears as an intense single isotropic line that overlaps several transitions from VO^{2+} . The spectroscopic parameters calculated from the simulation of the EPR spectrum (Figure 2b blue line) for each center are shown in Table 2. The EPR spectrum was described by the axial spin Hamiltonian

$$\hat{H} = g_{\parallel} \beta B_z \hat{S}_z + g_{\perp} \beta (B_x \hat{S}_x + B_y \hat{S}_y) + A_{\parallel} \hat{S}_{zz} + A_{\perp} (\hat{S}_{xx} + \hat{S}_{yy}), \quad (1)$$

where g_{\parallel} and g_{\perp} are the main components of the g tensor, A_{\parallel} and A_{\perp} are the main components of the hyperfine tensor, B_i , S_i , and I_i are the projections of the external magnetic field strength, electronic ($S = 1/2$), and nuclear ($I = 1$) spins, respectively, onto the $i = \{x, y, z\}$ coordinate axis, and β is the Bohr magneton. As seen from the equation, the direction of quantities with the index \perp correspond to the location in the xy plane, while the quantities with the index \parallel are directed along the z axis (Figure 2a).

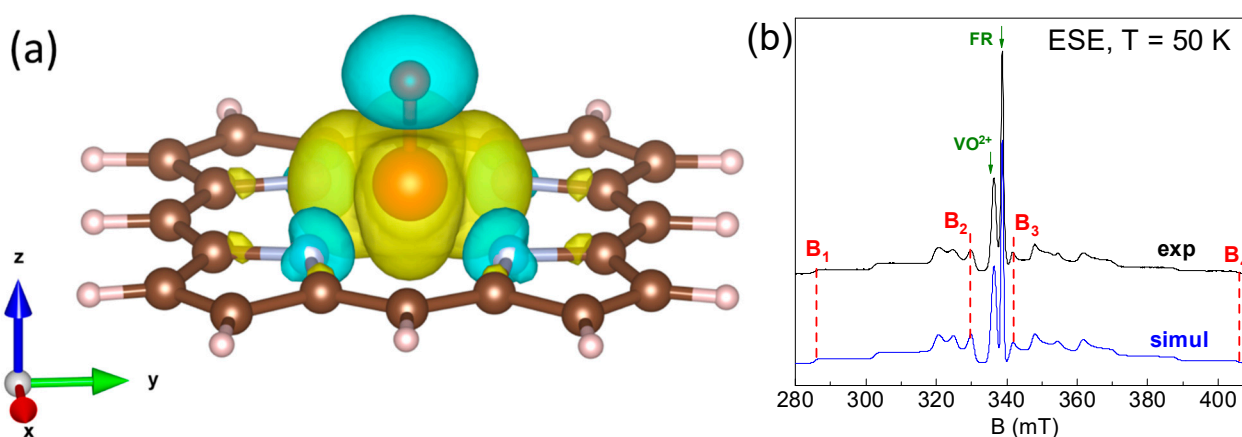


Figure 2. (a) Schematic representation of a vanadyl porphyrin molecule with the main axis of the VO^{2+} complex (see paper [35] for details), (b) EPR spectra of the Athabasca oil sands obtained in the pulsed mode (exp) with corresponding simulation (sim) in the assumption of the axial symmetry for ^{51}V . Signals belonging to FR and VO^{2+} are marked as well as the magnetic field values B_1 – B_4 for which HYSCORE measurements were performed.

Table 2. EPR spin-Hamiltonian parameters for the intrinsic for asphaltenes VP (VO^2) and FR.

	g_{\perp}	g_{\parallel}	A_{\perp}	A_{\parallel}
VO^{2+}	1.9868	1.965	158 MHz	472 MHz
FR	$g_{\text{iso}}=2.0038$		-	-

The fitting results (g-factors and hyperfine interaction constants, see Table 2) are in agreement with the results of previous works [36] on the study of asphaltenes samples from another oilfield. No HFI with other nuclei can be observed in the EPR spectrum.

The asphaltene sample under study is a powder material (with the orientational disorder). As mentioned above, in the HYSCORE spectra, the observation of HFIs from various magnetic nuclei is expected. In a powder spectrum, where all particle orientations with respect to the external magnetic field B_0 are equally probable, we would observe weakly unresolved lines with inhomogeneous broadening. However, as seen in Figure 2b for the EPR spectrum, due to the pronounced anisotropic HFI for VP, it is possible to identify the canonical positions (perpendicular and parallel directions) for further orientation-selective measurements by the HYSCORE method. Thus, we get rid of signal broadening due to angular spread and obtain crystal-like spectra. We have carried out several HYSCORE measurements that correspond to different orientations of the VP relative to B_0 . These positions are marked on the EPR spectrum (Figure 2b).

Figure 3a shows that the decays of the transverse magnetization of the VP with the modulations (ESEEM) measured in the magnetic field denoted as VO^{2+} in Figure 2b by increasing the time τ between $\pi/2$ and π pulses. The main condition for the observation of nuclear modulations is the presence of anisotropic hyperfine interaction of the paramagnetic center with the surrounding magnetic nuclei. The frequency ν and amplitude (depth) of the modulation for each center may differ markedly. This may be caused by a different ionic environment, the degree of anisotropy of the hyperfine interaction, and the orientation of the center relative to the magnetic field. The oscillation frequency is determined by ν_{Larmor} , which depends on the type of nucleus (the value of the gyromagnetic ratio γ) and the presence of various interactions (hyperfine or quadrupole).

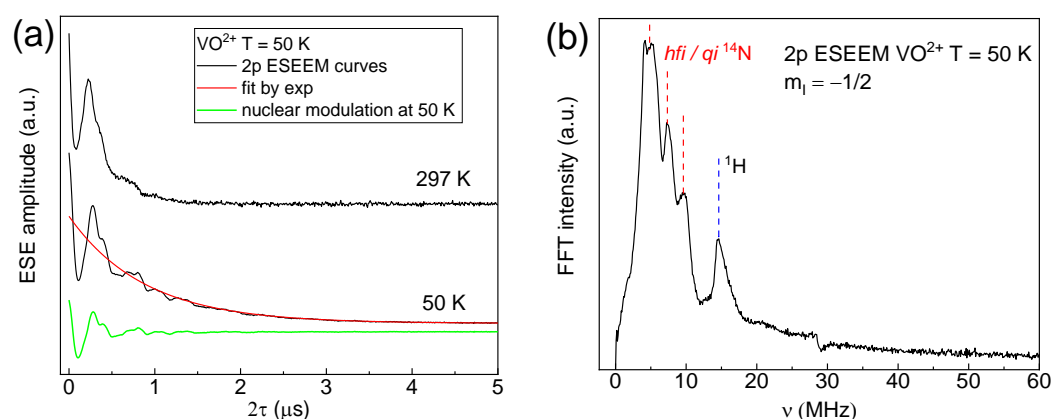


Figure 3. (a) The decay curves in time domain of the transverse magnetization of the VP complex measured in the magnetic field denoted as VO^{2+} in Figure 2 at two temperatures (50 K and 297 K) with the corresponding fitting for $T = 50$ K as a monoexponential function with $T_2 = 880$ ns, (b) The ESEEM spectrum for $T = 50$ K in the frequency domain after the Fourier transform.

The Fourier spectrum of the ESEEM signal from the VP is shown in Figure 3b. The line at 14.8 MHz (Figure 3b) belongs to the 1H hydrogen nuclei ($\gamma/2\pi = 42.58$ MHz/T) framing the VP. Intense low-frequency resonance lines correspond to vanadium ^{51}V ($\gamma/2\pi = 7.05$ MHz/T) and nitrogen ^{14}N ($\gamma/2\pi = 3.077$ MHz/T) nuclei. As seen, the ESEEM spectrum allows us to determine the type of core surrounded by a paramagnetic center. Unfortunately, the presence of hyperfine and quadrupole interactions from ^{14}N nitrogen nuclei, as well as the presence of cross frequencies (the sum and difference typical of a two-pulse ESEEM), leads to complications of the spectrum. It became difficult to attribute the lines to certain nuclear transitions unambiguously and read out the values of the electron–nuclear interactions. HYSCORE measurements can help to resolve emerging problems.

The values of B_0 for the HYSCORE measurements (Figure 2b) were chosen as the most orientationally “pure”, i.e., the centers in canonical orientations should contribute to the

EPR signal at these B_0 values. Nevertheless, it is not possible to achieve precise positioning due to the fact that the width of each hyperfine transition line has a finite value. In this work, pulse sequences are used with the duration of the exciting π pulse of 32 ns. Each individual pulse has its own excitation spectrum in the frequency range. The excitation range was estimated as the first Fourier harmonic that, for the rectangular pulses used in this work, was equal to ≈ 3 MHz (≈ 1.1 mT). This value is enough to cover the EPR signal at a certain canonical orientation (perpendicular or parallel).

The studied samples are powders. Consequently, the EPR line broadening mechanism is caused mainly by an inhomogeneous contribution due to angular dispersion. Overlapping of the pulse excitation spectrum of the hyperfine EPR absorption component and inhomogeneous line broadening leads to the fact that one effectively detects the HYSORE spectra in the intermediate orientation of nanocrystals. The overlap of the pulse excitation spectrum of most of the EPR spectrum leads (1) to an increase in the signal; (2) to an increase in the probability of forbidden transitions that enhances HYSORE.

The HYSORE spectra in perpendicular orientation (B_2 and B_3) are shown in Figure 4. In the right quadrant (+,+), where nuclei with a weak bond ($A < 2\nu$) are present, signals from nitrogen ^{14}N , vanadium ^{51}V , and hydrogen ^1H nuclei were recorded. There are no additional splittings for ^1H and ^{14}N nuclei; however, for ^{51}V , a hyperfine structure is detected with $A = 4.7$ MHz. Considering that the EPR spectrum of vanadium exceeds hundreds of MHz, the unresolved signal from nitrogen indicates that these nuclei belong to the far environment (for example, the second coordination sphere) of VO^{2+} . In the left quadrant, there is a signal from one-quantum transitions of nitrogen nuclei with the strong HFI binding ($A = 8.3$ – 8.6 MHz). These signals belong to the near nuclear environment. The remaining signals located on the right diagonal and marked in gray are artifacts caused by nonideal $\pi/2$ and π pulses.

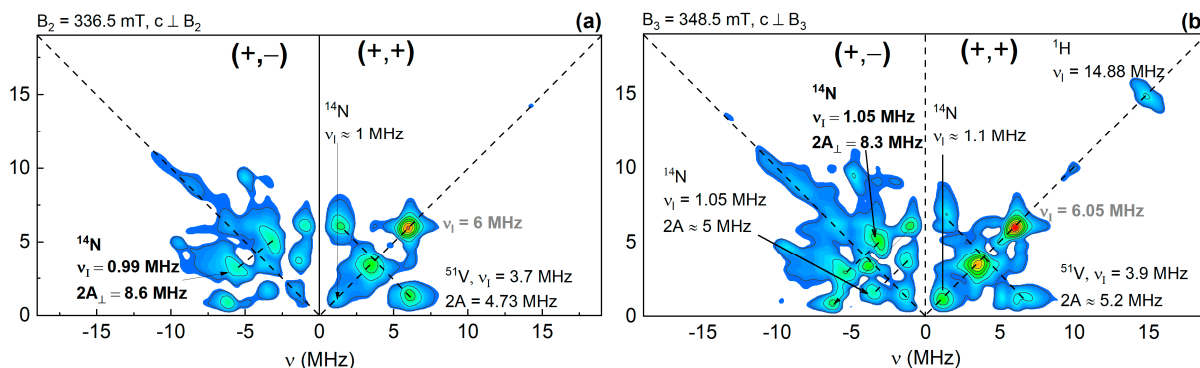


Figure 4. HYSORE spectra in the perpendicular orientation of the VP complex where (a) $B_2 = 336.5$ mT and (b) $B_3 = 348.5$ mT (see also Figure 2b).

In the HYSORE spectra, signals with weak hyperfine coupling appear in the right quadrant, where the Larmor frequency is greater than the HFI value A . In the left quadrant, signals from magnetic nuclei ($I > 0$) with strong hyperfine coupling are displayed. The values of the electron–nuclear interaction of their HYSORE spectra were determined in accordance with the two-dimensional spectrum and the arrangement scheme depicted in Figure 2b. The values of ν_{Larmor} of magnetic nuclei depend on two main quantities: the gyromagnetic ratio constant γ_n , indicating the nature and type of the nucleus, as well as the magnitude of the external magnetic field B_0 . Figures 4 and 5 show all Larmor frequencies, which have different values due to changes in B_0 .

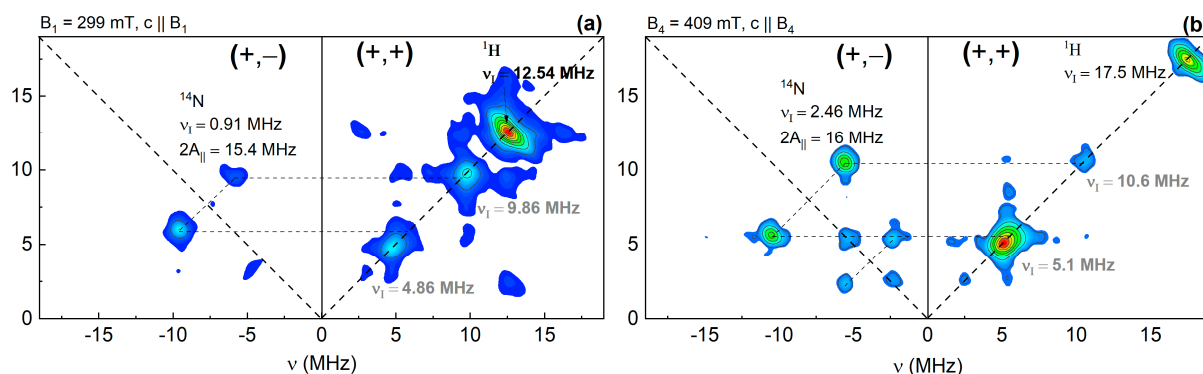


Figure 5. HYSORE spectra in parallel orientation of the VO^{2+} skeleton where (a) $B_1 = 299$ mT and (b) $B_3 = 409$ mT (see also Figure 2b).

Hyperfine interaction in HYSORE spectra can be assigned to two contributions: the isotropic contact Fermi component, A_{iso} , and anisotropic dipole–dipole term, A_{dd} . The anisotropic dipole–dipole contribution has an angular dependence. The relationship between the various HFI components can be expressed as follows

$$A = A_{\text{dd}} \left(3 \cos^2 \theta - 1 \right) + A_{\text{iso}} \text{ (HFI value)} \quad (2)$$

$$A_{\parallel} = 2A_{\text{dd}} + A_{\text{iso}} \text{ (parallel component)} \quad (3)$$

$$A_{\perp} = -A_{\text{dd}} + A_{\text{iso}} \text{ (perpendicular component)}, \quad (4)$$

where θ is the angle between the directions of B_0 and z , r is an interatomic distance between the magnetic spins.

Figure 5 shows spectra for parallel orientation (B_1 and B_4). There are no obvious signs of nitrogen and vanadium nuclei ^{51}V in the right quadrant, except for an intense signal from ^1H . For the left quadrant, the signals from the nitrogen nuclei are still present, but they are recorded exclusively from two-quantum transitions with the selection rule $\Delta m_I = \pm 2$, located at twice the Larmor frequency of ^{14}N and with a splitting of $2A$ due to the additional quadrupole interaction for ^{14}N [35].

The presence of two quantum transitions may indicate a strong quadrupole coupling, which leads to entanglement of the spin nuclear sublevels. Electronic spin states form wave functions, which in intermediate orientations form shifted states. The presence of mixed wave functions is a prerequisite for the occurrence of electronic forbidden transitions and the observation of HYSORE signals. However, this entanglement due to the strong quadrupole coupling can lead to forbidden nuclear transitions with a change in the projection of the nuclear quantum number by two. Additionally, the doubled frequencies can be caused by the presence of two equivalent nuclei with the same values of hyperfine interaction near the paramagnetic center under study. Such a structure gives a doubled frequency in the HYSORE spectrum.

From Equations (3) and (4), one can determine the values of the isotropic and dipole–dipole contributions to the ^{14}N HFI as

$$A_{\text{iso}} = \frac{A_{\parallel} + 2A_{\perp}}{3} = \frac{15.4 \text{ MHz} + 2 \times 8.6 \text{ MHz}}{3} = 8.3 \text{ MHz},$$

$$A_{\text{dd}} = \frac{A_{\parallel} - A_{\perp}}{3} = \frac{7.7 \text{ MHz} - 8.6 \text{ MHz}}{3} = -0.3 \text{ MHz}.$$

HFI isotropic value is determined by the electron density on the nucleus. The electron density can be calculated theoretically by using density functional theory (DFT), for example [5], and it depends on the structure of the vanadium complex. From the value

of the electron–nuclear dipole–dipole interaction (between the electron shell of vanadium and the nearest nitrogen nuclei), an interatomic distance between the magnetic spins can be estimated [36] that is, in our case (point–dipole approximation) is $r \approx 2.1 \text{ \AA}$. DFT calculations [5,35] give the value of $r = 2.069 \text{ \AA}$.

4. Conclusions

In this work, the capabilities of EPR spectroscopy for the analysis of electron–nuclear interactions of intrinsic magnetic species surrounding paramagnetic vanadyl porphyrins for oil asphaltenes without dilution or other specific sample preparation were studied. The main spectroscopic parameters of the spin Hamiltonian ($g_{\perp} = 1.9868$, $g_{\parallel} = 1.965$, $A_{\perp} = 158 \text{ MHz}$ and $A_{\parallel} = 472 \text{ MHz}$) were determined. The values of the isotropic ($A_{\text{iso}} = 8.3 \text{ MHz}$) and dipole–dipole ($A_{\text{dd}} = -0.3 \text{ MHz}$) contributions with the ^{14}N HFI were determined. From A_{dd} , an interatomic distance between the vanadium and the nearest nitrogen nuclei ($r \approx 2.1 \text{ \AA}$) is estimated.

The HYSORE method made it possible to resolve the contributions from various types of hyperfine interaction and determine the values of the hyperfine interaction of the electron magnetic moment of VP with the surrounding nuclei such as ^1H , ^{14}N , and ^{51}V . The proven approach can be used to study other petroleum systems. The obtained HFI data can serve as a reference to follow their potential changes under the external treatment.

Author Contributions: The idea of the experiment belongs to M.R.G. EPR and HYSORE measurements were performed by F.F.M., G.V.M. and M.A.S. The discussion of the obtained results was performed by G.V.M., F.F.M. and M.R.G. wrote the draft version of the paper. All authors have read and agreed to the published version of the manuscript.

Funding: This work was supported by RSF grant 21-73-30023.

Data Availability Statement: Data can be available upon request from the authors.

Conflicts of Interest: The authors declare no conflict of interest.

References

1. Yakubov, M.; Abilova, G.; Tazeeva, E.; Yakubova, S.; Tazeev, D.; Mironov, N.; Milordov, D. A Comparative Analysis of Vanadyl Porphyrins Isolated from Resins of Heavy Oils with High and Low Vanadium Content. *Processes* **2021**, *9*, 2235. [[CrossRef](#)]
2. Gotico, P.; Halime, Z.; Aukauloo, A. Recent Advances in Metalloporphyrin-Based Catalyst Design towards Carbon Dioxide Reduction: From Bio-Inspired Second Coordination Sphere Modifications to Hierarchical Architectures. *Dalton Trans.* **2020**, *49*, 2381–2396. [[CrossRef](#)] [[PubMed](#)]
3. Devatha, C.P.; Vishnu Vishal, A.; Purna Chandra Rao, J. Investigation of Physical and Chemical Characteristics on Soil Due to Crude Oil Contamination and Its Remediation. *Appl. Water Sci.* **2019**, *9*, 89. [[CrossRef](#)]
4. Yakubov, M.R.; Milordov, D.V.; Yakubova, S.G.; Abilova, G.R.; Sinyashin, K.O.; Tazeeva, E.G.; Borisova, U.U.; Mironov, N.A.; Morozov, V.I. Vanadium and Paramagnetic Vanadyl Complexes Content in Asphaltenes of Heavy Oils of Various Productive Sediments. *Pet. Sci. Technol.* **2017**, *35*, 1468–1472. [[CrossRef](#)]
5. Biktagirov, T.; Gafurov, M.; Mamin, G.; Gracheva, I.; Galukhin, A.; Orlinkii, S. In Situ Identification of Various Structural Features of Vanadyl Porphyrins in Crude Oil by High-Field (3.4 T) Electron–Nuclear Double Resonance Spectroscopy Combined with Density Functional Theory Calculations. *Energy Fuels* **2017**, *31*, 1243–1249. [[CrossRef](#)]
6. Gafurov, M.R.; Gracheva, I.N.; Mamin, G.V.; Ganeeva, Y.M.; Yusupova, T.N.; Orlinkii, S.B. Study of Organic Self-Assembled Nanosystems by Means of High-Frequency ESR/ENDOR: The Case of Oil Asphaltenes. *Russ. J. Gen. Chem.* **2018**, *88*, 2374–2380. [[CrossRef](#)]
7. Asaoka, S.; Nakata, S.; Shiroto, Y.; Takeuchi, C. *Asphaltene Cracking in Catalytic Hydrotreating of Heavy Oils. 2. Study of Changes in Asphaltene Structure during Catalytic Hydroprocessing*; ACS Publications: Washington, DC, USA, 1983. [[CrossRef](#)]
8. Mironov, N.A.; Milordov, D.V.; Abilova, G.R.; Yakubova, S.G.; Yakubov, M.R. Methods for Studying Petroleum Porphyrins (Review). *Pet. Chem.* **2019**, *59*, 1077–1091. [[CrossRef](#)]
9. Djimasbe, R.; Varfolomeev, M.A.; Al-muntaser, A.A.; Yuan, C.; Suwaid, M.A.; Feoktistov, D.A.; Rakhmatullin, I.Z.; Milovankin, A.A.; Murzakhanov, F.; Morozov, V.; et al. Deep Insights into Heavy Oil Upgrading Using Supercritical Water by a Comprehensive Analysis of GC, GC–MS, NMR, and SEM–EDX with the Aid of EPR as a Complementary Technical Analysis. *ACS Omega* **2021**, *6*, 135–147. [[CrossRef](#)]
10. Trukhan, S.N.; Kazarian, S.G.; Martyanov, O.N. Electron Spin Resonance of Slowly Rotating Vanadyls—Effective Tool to Quantify the Sizes of Asphaltenes in Situ. *Energy Fuels* **2017**, *31*, 387–394. [[CrossRef](#)]

11. Imran, M.; Ramzan, M.; Qureshi, A.K.; Khan, M.A.; Tariq, M. Emerging Applications of Porphyrins and Metalloporphyrins in Biomedicine and Diagnostic Magnetic Resonance Imaging. *Biosensors* **2018**, *8*, 95. [[CrossRef](#)]
12. Trukhan, S.N.; Yakushkin, S.S.; Martyanov, O.N. Fine-Tuning Simulation of the ESR Spectrum—Sensitive Tool to Identify the Local Environment of Asphaltenes In Situ. *J. Phys. Chem. C* **2022**, *126*, 10729–10741. [[CrossRef](#)]
13. Mannikko, D.; Stoll, S. Vanadyl Porphyrin Speciation Based on Submegahertz Ligand Proton Hyperfine Couplings. *Energy Fuels* **2019**, *33*, 4237–4243. [[CrossRef](#)]
14. McKenna, A.M.; Chacón-Patiño, M.L.; Salvato Vallverdu, G.; Bouyssiere, B.; Giusti, P.; Afonso, C.; Shi, Q.; Combariza, M.Y. Advances and Challenges in the Molecular Characterization of Petroporphyrins. *Energy Fuels* **2021**, *35*, 18056–18077. [[CrossRef](#)]
15. Sarkar, T.K.; Saraswat, V.; Mitra, R.K.; Obot, I.B.; Yadav, M. Mitigation of Corrosion in Petroleum Oil Well/Tubing Steel Using Pyrimidines as Efficient Corrosion Inhibitor: Experimental and Theoretical Investigation. *Mater. Today Commun.* **2021**, *26*, 101862. [[CrossRef](#)]
16. Jumina, J.; Kurniawan, Y.S.; Siswanta, D.; Purwono, B.; Zulkarnain, A.K.; Winarno, A.; Waluyo, J.; Ahmad, J.S.M. The Origin, Physicochemical Properties, and Removal Technology of Metallic Porphyrins from Crude Oils. *Indones. J. Chem.* **2021**, *21*, 1023–1038. [[CrossRef](#)]
17. Zhao, X.; Xu, C.; Shi, Q. Porphyrins in Heavy Petroleum: A Review. In *Structure and Modeling of Complex Petroleum Mixtures*; Xu, C., Shi, Q., Eds.; Structure and Bonding; Springer International Publishing: Cham, Switzerland, 2016; pp. 39–70. [[CrossRef](#)]
18. Gafurov, M.R.; Ponomarev, A.A.; Mamin, G.V.; Rodionov, A.A.; Murzakhanov, F.F.; Arash, T.; Orlinskii, S.B. Application of Pulsed and High-Frequency Electron Paramagnetic Resonance Techniques to Study Petroleum Disperse Systems. *Georesursy* **2020**, *22*, 2–14. [[CrossRef](#)]
19. Gafurov, M.; Mamin, G.; Gracheva, I.; Murzakhanov, F.; Ganeeva, Y.; Yusupova, T.; Orlinskii, S. High-Field (3.4 T) ENDOR Investigation of Asphaltenes in Native Oil and Vanadyl Complexes by Asphaltene Adsorption on Alumina Surface. *Geofluids* **2019**, *2019*, e3812875. [[CrossRef](#)]
20. Murzakhanov, F.F.; Mamin, G.V.; Goldberg, M.A.; Knotko, A.V.; Gafurov, M.R.; Orlinskii, S.B. EPR of Radiation-Induced Nitrogen Centers in Hydroxyapatite: New Approaches to the Study of Electron-Nuclear Interactions. *Russ. J. Coord. Chem.* **2020**, *46*, 729–737. [[CrossRef](#)]
21. Murzakhanov, F.F.; Mamin, G.V.; Orlinskii, S.B.; Gerstmann, U.; Schmidt, W.G.; Biktagirov, T.; Aharonovich, I.; Gottscholl, A.; Sperlich, A.; Dyakonov, V.; et al. Electron–Nuclear Coherent Coupling and Nuclear Spin Readout through Optically Polarized VB–Spin States in HBN. *Nano Lett.* **2022**, *22*, 2718–2724. [[CrossRef](#)]
22. Roessler, M.M.; Salvadori, E. Principles and Applications of EPR Spectroscopy in the Chemical Sciences. *Chem. Soc. Rev.* **2018**, *47*, 2534–2553. [[CrossRef](#)]
23. Gourier, D.; Delpoux, O.; Bonduelle, A.; Binet, L.; Ciofini, I.; Vezin, H. EPR, ENDOR, and HYSORE Study of the Structure and the Stability of Vanadyl–Porphyrin Complexes Encapsulated in Silica: Potential Paramagnetic Biomarkers for the Origin of Life. *J. Phys. Chem. B* **2010**, *114*, 3714–3725. [[CrossRef](#)] [[PubMed](#)]
24. Ben Tayeb, K.; Delpoux, O.; Barbier, J.; Marques, J.; Verstraete, J.; Vezin, H. Applications of Pulsed Electron Paramagnetic Resonance Spectroscopy to the Identification of Vanadyl Complexes in Asphaltene Molecules. Part 1: Influence of the Origin of the Feed. *Energy Fuels* **2015**, *29*, 4608–4615. [[CrossRef](#)]
25. Strausz, O.P.; Lown, E.M. *The Chemistry of Alberta Oil Sands, Bitumens, and Heavy Oils*; Alberta Energy Research Institute (AERI): Calgary, AB, Canada, 2003.
26. Elofson, R.M.; Schulz, K.F.; Hitchon, B. Geochemical Significance of Chemical Composition and ESR Properties of Asphaltenes in Crude Oils from Alberta, Canada. *Geochim. Cosmochim. Acta* **1977**, *41*, 567–580. [[CrossRef](#)]
27. Niizuma, S.; Iwaizumi, M.; Strausz, O.P. ENDOR [electron nuclear double resonance] study of free radicals in Athabasca asphaltene. *AOSTRA J. Res. Alta. Oil Sands Technol. Auth. Can.* **1991**, *7*, 217–223.
28. Elkahky, S.; Lagat, C.; Sarmadivaleh, M.; Barifcani, A. A Comparative Study of Density Estimation of Asphaltene Structures Using Group Contribution Methods and Molecular Dynamic Simulations for an Australian Oil Field. *J. Pet. Explor. Prod. Technol.* **2019**, *9*, 2699–2708. [[CrossRef](#)]
29. Gray, M.R.; Chacón-Patiño, M.L.; Rodgers, R.P. Structure–Reactivity Relationships for Petroleum Asphaltenes. *Energy Fuels* **2022**, *36*, 4370–4380. [[CrossRef](#)]
30. Ganeeva, Y.M.; Barskaya, E.E.; Okhotnikova, E.S.; Yusupova, T.N. Features of the Composition of Compounds Trapped in Asphaltenes of Oils and Bitumens of the Bavly Oil Field. *Energy Fuels* **2021**, *35*, 2493–2505. [[CrossRef](#)]
31. Nguyen, M.T.; Nguyen, D.L.T.; Xia, C.; Nguyen, T.B.; Shokouhimehr, M.; Sana, S.S.; Grace, A.N.; Aghbashlo, M.; Tabatabaei, M.; Sonne, C.; et al. Recent Advances in Asphaltene Transformation in Heavy Oil Hydroprocessing: Progress, Challenges, and Future Perspectives. *Fuel Process. Technol.* **2021**, *213*, 106681. [[CrossRef](#)]
32. Prisner, T.; Rohrer, M.; MacMillan, F. Pulsed EPR spectroscopy: Biological applications. *Annu. Rev. Phys. Chem.* **2001**, *52*, 279–313. [[CrossRef](#)]
33. Lund, A.; Shiotani, M.; Shimada, S. *Principles and Applications of ESR Spectroscopy*; Springer Science & Business Media: Berlin/Heidelberg, Germany, 2011.
34. Stoll, S.; Schweiger, A. EasySpin, a Comprehensive Software Package for Spectral Simulation and Analysis in EPR. *J. Magn. Reson.* **2006**, *178*, 42–55. [[CrossRef](#)]

35. Gracheva, I.N.; Gafurov, M.R.; Mamin, G.V.; Biktagirov, T.B.; Rodionov, A.A.; Galukhin, A.V.; Orlinskii, S.B. ENDOR Study of Nitrogen Hyperfine and Quadrupole Tensors in Vanadyl Porphyrins of Heavy Crude Oil. *Magn. Reson. Solids Electron. J.* **2016**, *18*, 16102.
36. Mamin, G.V.; Gafurov, M.R.; Yusupov, R.V.; Gracheva, I.N.; Ganeeva, Y.M.; Yusupova, T.N.; Orlinskii, S.B. Toward the Asphaltene Structure by Electron Paramagnetic Resonance Relaxation Studies at High Fields (3.4 T). *Energy Fuels* **2016**, *30*, 6942–6946. [[CrossRef](#)]